ACS APPLIED MATERIALS & INTERFACES

Research Article

Cite This: ACS Appl. Mater. Interfaces 2018, 10, 350−360

www.acsami.org

One-Step in Situ Detection of miRNA-21 Expression in Single Cancer Cells Based on Biofunctionalized MoS_2 Nanosheets

Gerile Oudeng,[†,‡] Manting Au,[†] Jingyu Shi,[†,‡] Chunyi Wen,*[,†] and Mo Yang*[,†,‡]

[†]Department of Biomedical Engineering, The Hong Kong Polytechnic University, Hong Kong, P. R. China

[‡]The Hong Kong Polytechnic University Shenzhen Research Institute, Shenzhen 518057, P. R. China

Supporting Information

ABSTRACT: Here, we report the one-step in situ detection of targeted miRNAs expression in single living cancer cells via MoS_2 nanosheet-based fluorescence on/off probes. The strategy is based on the folic acid (FA)−poly(ethylene glycol)-functionalized MoS_2 nanosheets with adsorbed dye-labeled single-stranded DNA (ssDNA). Once the nanoprobes are internalized into cancer cells, the hybridization between the probes and target miRNA results in the detachment of dye-labeled ssDNA from MoS_2 nanosheets surface, leading to the green fluorescence recovery. In this nanoprobe, MoS_2 nanosheets offer advantages of high fluorescence quenching efficiency and extremely low toxicity. The FA conjugation could protect the probes and improve cancer cell transfection efficiency. The ability of this nanoprobe for endogenous miRNA detection in single living cancer cells is demonstrated for two types of cancer cells with different miRNA-21 expressions (MCF-7 and Hela cells). This functionalized MoS_2 nanosheet-based nanoprobes could provide a sensitive and real-time detection of intracellular miRNA detection platform.

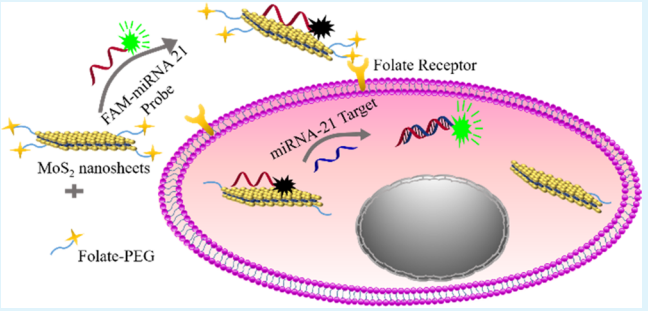

KEYWORDS: *miRNAs, in situ detection, MoS_2 nanosheets, fluorescence resonance energy transfer (FRET), cancer cells*

1. INTRODUCTION

MicroRNAs (miRNAs) are short noncoding sequences with 19−25 nucleotides.[1] They can regulate the diverse gene expression by inhibiting gene translation or enhancing the mRNA degradation in the post-transcriptional level.[2] miRNAs work in a relatively early and upstream level in the molecular pathways of cells, and many of them express specifically in diverse normal cells, tumors, or viruses.[3] miRNAs are also reported to be closely related to drug resistance of cancer cells.[4,5] Thus, miRNA is becoming a potential "seeded player" for molecular biomarker in early prediction and indication of tumorigenesis or metastasis. For example, in a perspective view, miRNA-21 was reported to have abnormally high expression in many kinds of cancer cells lines, involving breast cancer, cervical cancer, lung cancer, pancreatic cancer, and so on, and it was described closely related to the chemotherapeutic sensitivity of tumors.[6−8]

The current methods for miRNA detection are mainly based on end-point techniques, such as qualitative reverse transcription polymerase chain reaction (qRT-PCR),[9] northern blotting,[10,11] and microarray,[12,13] which can sensitively measure miRNAs. However, these methods suffer from the need of a large amount of cell samples, time-consuming process, and end-point checking feature. Due to the low-level expression of miRNAs in cells, the rapid and sensitive detection of miRNAs in living cells is still a challenge. Accordingly, reliable and sensitive detection of miRNAs in living cells is needed for early diagnosis and therapy.[14,15]

Fluorescence resonance energy transfer (FRET) is a sensitive technique to detect biomolecules on the basis of the energy transfer from donor to acceptor.[16−19] Recently, graphene and graphene-like two-dimensional nanomaterials, including graphene oxide (GO), graphitic carbon nitride (g-C_3N_4) nanosheets, and transition-metal dichalcogenides, such as molybdenum disulfide (MoS_2), have been used as efficient fluorescence quenchers due to their large surface area and unique optical properties.[20−27] Particularly, MoS_2 nanosheets have aroused a lot of interests for intracellular applications, such as intracellular adenosine triphosphate detection, gene delivery, cellular imaging, and therapy due to their low cytotoxicity even compared to GO.[28−33] However, the possibility using MoS_2-based probes for intracellular miRNA detection has not been explored yet.

Herein, we report, for the first time, monitoring of endogenous miRNA expression via MoS_2 nanosheet-based nanoprobe, which could realize one-step in situ miRNA expression detection at single-cell level. For such purpose, folate-functionalized MoS_2 nanosheets immobilized with fluorescence-labeled ssDNA probes (ssDNA−MoS_2−PEG−

Received: November 28, 2017
Accepted: December 14, 2017
Published: December 14, 2017

DOI: 10.1021/acsami.7b18102
ACS Appl. Mater. Interfaces 2018, 10, 350−360

FA) were prepared by covalently immobilizing FA on MoS_2 nanosheets via the lipoic acid−poly(ethylene glycol) ester (LA−PEG−NH_2) and $\pi-\pi$ stacking between the dye-labeled ssDNA probe and M_OS_2 nanosheets. As shown in Scheme 1,

Scheme 1. Schematic of ssDNA−MoS_2−PEG−FA Probe-Based FRET Platform for Intracellular miRNA-21 Detection

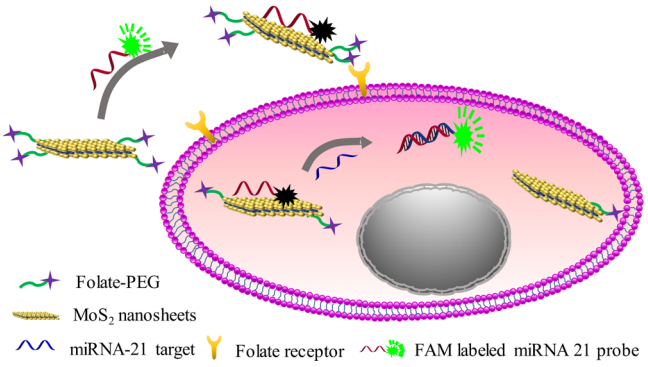

this fluorescence turn-on sensor is established by quenching the absorbed dye-labeled ssDNA probes on MoS_2 nanosheets to an "off" state due to the fluorescence resonance energy transfer (FRET) effect. The conjugated folate via LA−PEG linker could protect ssDNA probes and improve cancer cell targeting and internalization process. When ssDNA−MoS_2−PEG−FA nanoprobes are internalized by cancer cells, the higher binding force between target miRNA-21 and ssDNA probes leads to the rapid fluorescence recovery due to the detachment of dye-labeled ssDNA probes from MoS_2 nanosheets. With this simple strategy, we used this functionalized MoS_2 nanosheet-based nanoprobes for miRNA-21 detection in both cell-free system and inside living cancer cells with different expressions of miRNA-21. This platform can be a potential platform for in situ detection of intracellular miRNA in early diagnostics and treatment applications.

2. EXPERIMENTAL SECTION

2.1. Materials. MoS_2 material was purchased from Muke Nano Science and Technology Ltd., Nanjing, China. After sonication, MoS_2 nanosheets dispersion solution was dialyzed with a filter membrane with 3500D molecular weight cutoff (MWCO) for 1 day to eliminate lithium hydroxide (LiOH). Then, the dispersion was centrifuged at 2000 rpm for 5 min. All of the samples of miRNA-21, scrambled DNA, miRNA-20a, and target miRNA-21 were synthesized and purified by Sangon Biotech, Shanghai, China. The first three DNA sequences were modified with carboxyfluorescein (FAM) in the 5′ terminal. The sequences are described as follows: scrambled DNA probe (FAM-5′-TGC GCT CCT GGA CGT AGC CTT-3′), miRNA-20a (FAM-5′-FAM-TAA AGT GCT TAT AGT GCA GGT AG-3′), miRNA-21 probe (FAM-5′-TCA ACA TCA GTC TGA TAA GCT A-3′), and target miRNA-21 sequence (5′-UAG CUU AUC AGA CUG AUG UUG A-3′). All of the synthesized DNA sequences were dissolved in ultrapure water as stock solution and kept at −20 °C. Ethyl-3-(3-dimethyl-aminopropyl)carbodiimide (EDC) and *N*-hydroxysulfosuccinimide (sulfo-NHS) were purchased from Sigma-Aldrich. Folic acid was also purchased from Sigma-Aldrich. Lipoic acid−PEG−NH_2 (MW: 2000 Da) was purchased from ToYongBio Ltd., Shanghai, China, and stored at −20 °C. Dialysis bags (MWCO: 3500D and 1000D) and tubes (MWCO: 1000D) were purchased from GE Lifescience and stored at −4 °C. All of the cell culture reagents, including Dulbecco's modified Eagle's medium (DMEM) (high glucose), trypsin 0.25% ethylenediaminetetraacetic acid (EDTA), phosphate-buffered saline (PBS), fetal bovine serum (USA origin), 3-(4,5-dimethylthiazol-2-yl)-2,5-diphenyltetrazolium bromide (MTT), and penicillin/streptomycin, were purchased from Life Technologies Inc.

Agarose gel electrophoresis retardation assay was purchased from Biowest, Spain. The DNA ladder (M1100-50) was purchased from Solarbio Science & Technology Co. Ltd., Beijing, China. The main reagents for Western blotting, including radio-immunoprecipitation assay lysis buffer, protease inhibitor cocktail, β-actin, horseradish peroxidase-labeled goat antimouse IgG, and bicinchoninic acid protein assay kit, were purchased from Servicebio Technology Co. Ltd., China. Annexin V-FITC/PI Apoptosis Detection Kit for flow cytometry was purchased from NanJing KeyGen Biotech Co. Ltd., China. Molybdenum Standard for ICP TraceCERT was purchased from Sigma-Aldrich.

2.2. Characterization. The morphology and size of MoS_2 nanosheets were characterized using a JEOL-2100F transmission electron microscope installed with an Oxford Instruments EDS system (200 kV). The absorbance spectra of MoS_2 nanosheets were obtained with a UV−vis spectrophotometer (Ultrospec 2100 pro). Size distribution and ζ potential of MoS_2 nanosheets were determined at neutral pH with a Zetasizer Nano Z system (Malvern Instruments Ltd). Powder X-ray diffraction (XRD) pattern of MoS_2 nanosheets was obtained using an X-ray diffractometer (Rigaku SmartLab). Fourier transform infrared (FTIR) spectra of MoS_2 nanosheets and MoS_2−PEG−FA were acquired with a Bruker Vertex-70 FTIR spectrometer. Thermogravimetric analysis (TGA) was performed with a thermogravimetric analyzer (Netzch STA 449C, Jupiter). X-ray photoelectron spectra (XPS) for functionalization analysis were determined on an AXIS ULTRA DLD X-ray photoelectron spectrometer (Kratos, Tokyo, Japan)

2.3. MoS_2 FRET Nanoprobe Establishment. Folic acid (FA) was first conjugated with LA−PEG−NH_2 to form LA−PEG−FA following a previous protocol.[30,34] For this purpose, 0.15 mmol folic acid was dissolved in 2.5 mL of dimethyl sulfoxide (DMSO) for 8 h. FA solution was then added with 0.17 mmol EDC and 0.33 mmol NHS for activation. LA−PEG−NH_2 (0.15 mmol) was then added for reaction overnight. The final product was collected and dialyzed with a 1 kDa dialysis bag for 4−5 days, and dialysis water was changed every day to remove the organic solution and the excess reagent. The final product LA−PEG−FA was lyophilized using a ScanVac cs55-4 CoolSafe freeze dryer.

LA−PEG−FA was then conjugated on MoS_2 nanosheets to form MoS_2−PEG−FA complex. LA−PEG−FA (65 μg) powder was added into 0.6 mg of MoS_2 nanosheets dispersed in 1.2 mL of water. The mixture was sonicated for 20 min and stirred for 5 h. Then, the samples were filtered by 100 kDa MWCO filters and centrifuged to remove the extra LA−PEG−FA. The obtained MoS_2−PEG−FA complex was highly water-soluble and then stored in 4 °C for further usage.

In quenching efficiency experiment, FAM-labeled miRNA-21 probe with a fixed concentration of 30 nM was incubated with MoS_2−PEG−FA nanosheets in a series of concentrations (5−120 μg/mL) for 30 min at room temperature. Then, the fluorescence intensity was measured with 488 nm excitation wavelength. As control groups, FAM-labeled scRNA probes and FAM-labeled miRNA-20a probes were loaded with same amount under the same experimental conditions.

The stabilities of ssDNA carried by MoS_2 and MoS_2−PEG under DNase I treatment were evaluated through gel electrophoresis assay. Briefly, naked ssDNA, ssDNA−MoS_2, and ssDNA−MoS_2−PEG were incubated with DNase I (0.15 unit/μL) at 37 °C for 5 and 20 min, respectively. Naked ssDNA, ssDNA−MoS_2, and ssDNA−MoS_2−PEG without nuclease treatment were used as control groups. Samples of each group were stirred and loaded into the prepared agarose gel (3%) at 120 V for 30 min. After electrophoresis, the gel was stained with 0.5 μg/mL ethidium bromide (EtBr) and washed with water. The bands were visualized by Tanon 1600/1600R Gel Imaging System.

2.4. In Vitro miRNA Detection. For target detection, ssDNA−MoS_2−PEG−FA nanocomplex was incubated with a series of

DOI: 10.1021/acsami.7b18102
ACS Appl. Mater. Interfaces 2018, 10, 350−360

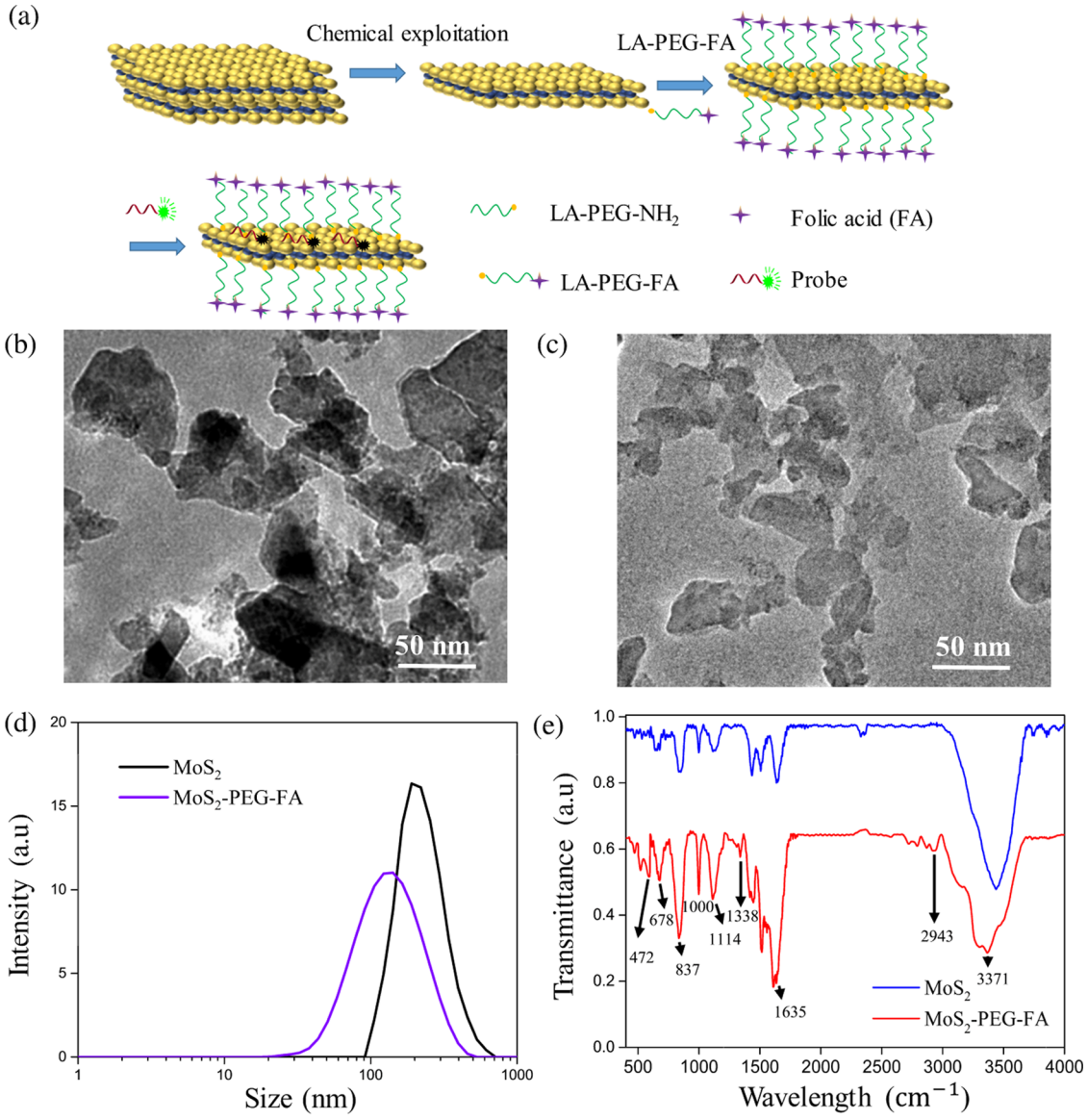

Figure 1. (a) Schematic of the preparation process of nanoprobes. (b) TEM image of synthesized MoS_2 nanosheets. (c) TEM image of synthesized MoS_2–PEG–FA. (d) Size distribution of MoS_2 nanosheets and MoS_2–PEG–FA. (e) FTIR spectra of MoS_2 nanosheets and MoS_2–PEG–FA.

concentrations of miRNA-21 target sequences from 10 to 50 nM. After 2 h incubation at 37 °C in the dark environment, the fluorescence signal of each sample was measured. To investigate the specificity, FAM-labeled scRNA probe and miRNA-20a probe were used with the same detection protocol. Fluorescence spectra of quenching and fluorescence recovery were recorded with an Edinburgh FLSP920 spectrophotometer equipped with a 450 W steady-state xenon lamp at room temperature.

2.5. Cell Culture and Cytotoxicity Assay. MCF-7 cells and Hela cells were cultured in a high-glucose medium containing 10% fetal bovine serum and 1% penicillin/streptomycin at 37 °C in 5% CO_2 atmosphere. For cell viability experiment, the cells were first seeded on a 96 well plate and medium was changed each day. MoS_2 nanosheets and the MoS_2–PEG–FA complex with a series of concentration from 0 to 200 μg/mL were added into the 96 well plate with a density of about 4.0×10^4 cells/well. After incubation with nanomaterials for 24 h, 10 μL of 12 mM MTT stock solution was added into each well and the cells were incubated at 37 °C in 5% CO_2 for 4 h. Then, the medium in each well was replaced with DMSO for another 10 min incubation in 37 °C. After sufficiently mixing, the absorbance of the samples was measured at 570 nm using a Tecan Infinite F200 microplate reader to evaluate the viability of the cells. The cell viability (%) was calculated as $(A_m/A_{control}) \times 100$, where A_m represents the absorbance at 570 nm of cells. The MCF-7 cells were cultured in 6 well plates with a density of 4.0×10^4/well and then incubated with MoS_2 (200 μg/mL) and MoS_2–PEG (200 μg/mL) for 24 h, respectively. Afterward, MCF-7 cells were treated with EDTA-free trypsin and washed with PBS. After further washing with PBS at 4 °C, the MCF-7 cells were resuspended with 200 μL of binding buffer and treated with 5 μL of Annexin V-FITC and 5 μL of propidium iodide in the dark environment for 15 min. The apoptosis of cells was analyzed with CytoFLEX (Beckman).

2.6. Western Blotting Analysis. The expression levels of surface folate receptor (FR) in MCF-7, Hela, NIH3T3, and HepG2 cell lines were determined by Western blotting assay. The protein samples were analyzed by 12% sodium dodecyl sulfate polyacrylamide gel electrophoresis and transferred to a poly(vinylidene difluoride) membrane. After electroblotting of the gels, the filters were blocked with 5% skimmed milk in Tris-buffered saline Tween-20 (TBST) buffer (0.1% Tween-20, 10 mM Tris–HCl, pH = 8) and then incubated with anti-FR protein monoclonal antibody at 4 °C overnight. After washing, the blots were incubated with 1:3000 diluted goat antimouse IgG monoclonal antibody in TBST buffer.

DOI: 10.1021/acsami.7b18102
ACS Appl. Mater. Interfaces 2018, 10, 350–360

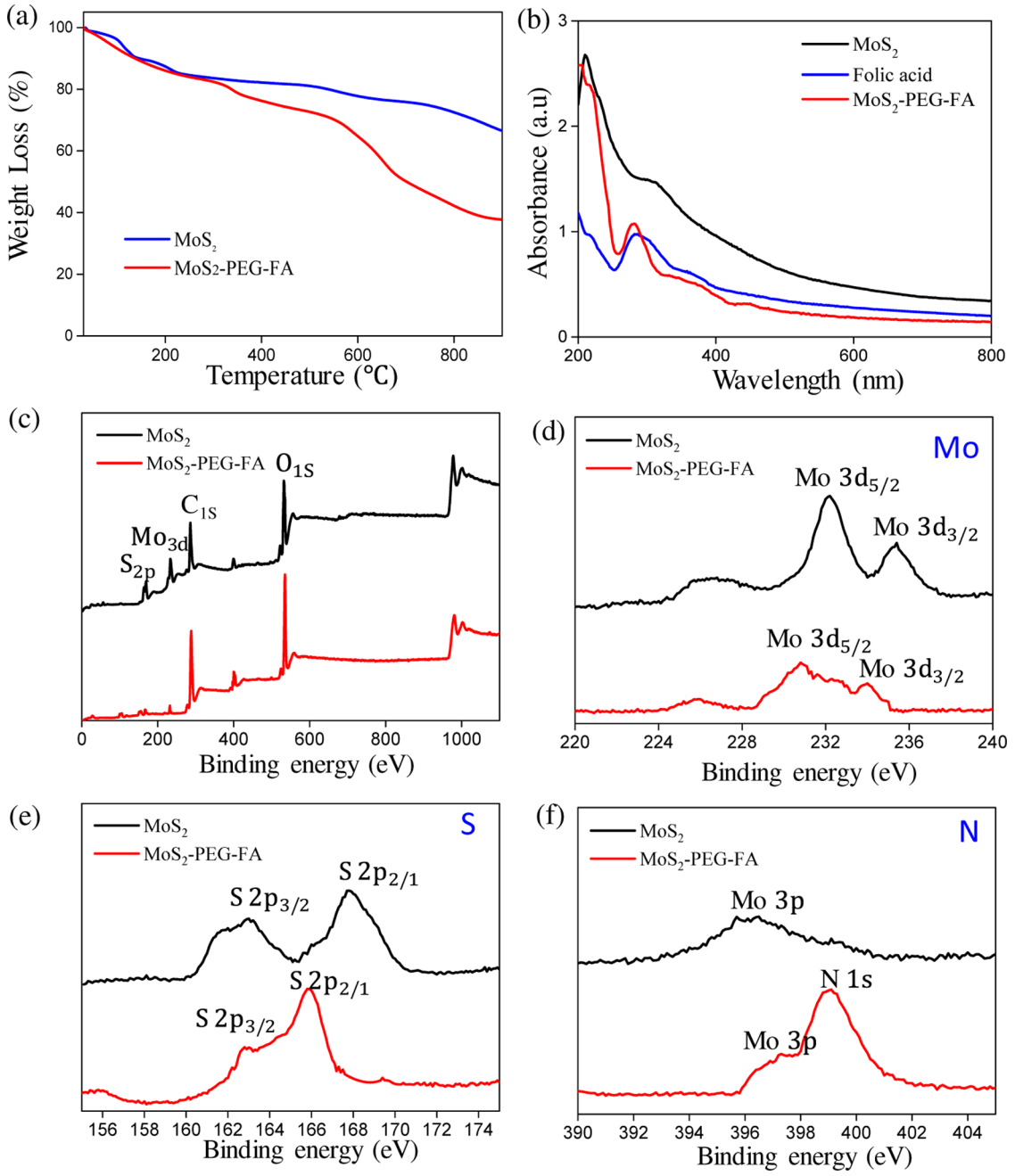

Figure 2. (a) TGA diagram of MoS_2 nanosheets and MoS_2−PEG−FA. (b) UV−vis spectra of MoS_2, FA, and MoS_2−PEG−FA. (c) Full XPS images of synthesized MoS_2 nanosheets and MoS_2−PEG−FA. High-resolution XPS images of (d) Mo 3d, (e) S 2p, and (f) N 1s.

Finally, the protein bands were visualized with enhanced chemiluminescence.

2.7. Inductively Coupled Plasma Mass Spectrometry (ICP-MS) Quantitative Analysis of Cellular Uptake. To quantitatively evaluate the effect of FA modification on cellular uptake of nanoprobes, four different kinds of cell lines (MCF-7, Hela, NIH3T3, and HepG2) were seeded with a density of 4.0×10^4/well at 75 cm^2 flask. The cells were incubated with MoS_2−PEG and MoS_2−PEG−FA (100 μg/mL) for 4 h. After incubation, the cells were washed with PBS three times and then digested with trypsin. The cell suspension was fixed in 2.5% glutaraldehyde and dehydrated with a series of ethanol concentrations. The collected cells were then dried in a vacuum desiccator and weighed. The cell samples were then dissolved by nitric acid solution and diluted by deionized water to 10 mL with indium (5 ppb) as the internal standard.[35,36] The concentration of Mo^{4+} was determined by an Agilent 7500ce inductively coupled plasma mass spectrometer (ICP-MS). The intensity ratios of the molecular Mo^{4+} ions to the internal standard Mo^{4+} ions were determined and plotted against molybdenum standard solution to generate a calibration curve (Figure S1).

2.8. Intracellular miRNA Monitoring. MCF-7 cells were first cultured in 75 cm^2 flask for 1 week with a cell density of 4.0×10^4 cells/mL. To monitor the endogenous miRNA-21 expression in MCF-7 cells and Hela cells, the cells were seeded into confocal dishes (35 mm) and cultured for 24 h at 37 °C in a 5% CO_2 environment. Then, ssDNA−MoS_2−PEG−FA complex of 100 μg/mL, which was confirmed with 90% cell viability and 92% quenching efficiency, was then loaded with FAM-labeled miRNA-21 probe and added into the confocal dishes. After 4 h incubation at 37 °C and 5% CO_2 environment, the cells were washed with PBS gently for confocal imaging with a Leica TCS SPE confocal microscope system. The excitation laser was set at 488 nm, and the green fluorescence signal

DOI: 10.1021/acsami.7b18102
ACS Appl. Mater. Interfaces 2018, 10, 350−360

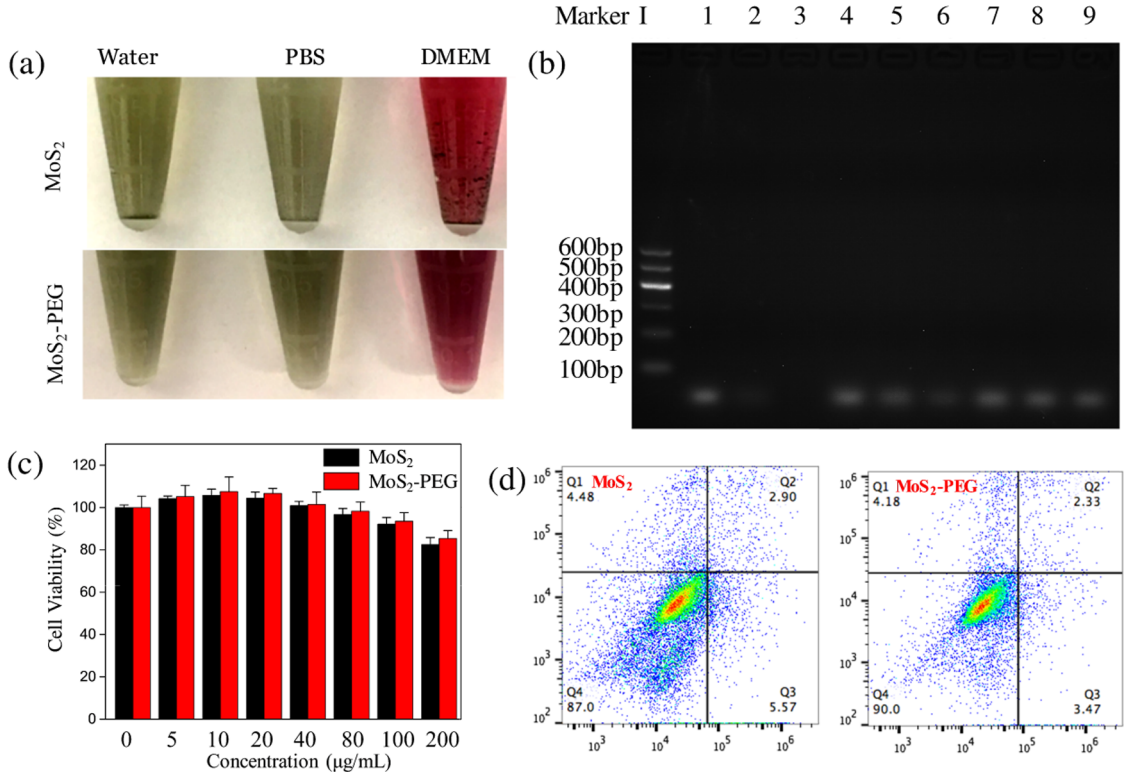

Figure 3. (a) Photos of MoS_2 nanosheets and MoS_2–PEG–FA complex distributed in water, PBS, and cell medium after 4 h of standing. (b) Gel electrophoresis of ssDNA, ssDNA–MoS_2, and ssDNA–MoS_2–PEG with and without DNase I treatment; lanes 1–3: ssDNA without DNase I, ssDNA treated with DNase I for 5 and 20 min; lanes 4–6: ssDNA–MoS_2 without DNase I, ssDNA–MoS_2 treated with DNase I for 5 and 20 min; lanes 7–9: ssDNA–MoS_2–PEG–FA without DNase I, ssDNA–MoS_2–PEG–FA treated with DNase I for 5 and 20 min. (c) Cell viability analysis of MCF-7 cells incubated with MoS_2 nanosheets and MoS_2–PEG for 24 h by MTT assay. (d) Cell apoptosis analysis of MCF-7 cells incubated with MoS_2 nanosheets (left) and MoS_2–PEG (right) for 24 h by flow cytometry.

was collected within the range of 505–540 nm under the same conditions. Cell images in bright field, fluorescence, and overlap of the two fields were captured and analyzed. Single-cell fluorescence images were then analyzed with ImageJ software. Flow cytometry was used to quantitatively analyze fluorescence recovery signals of multiple cells. The cell samples were first incubated with nanoprobes and then collected with trypsin followed by washing with PBS several times. The fluorescence recovery signals of multiple cells were then analyzed with a CytoFLEX flow cytometer (Beckman) fitted with a 488 nm excitation laser.

3. RESULTS AND DISCUSSION

3.1. Synthesis of ssDNA–MoS_2–PEG–FA Probes. The proposed ssDNA–MoS_2–PEG–FA nanoprobes provide a rapid and sensitive strategy for intracellular miRNA-21 detection in living cancer cells. As shown in Figure 1a, MoS_2 nanosheets were first prepared by a simple sonication-assisted exfoliation approach from bulk MoS_2 powder. XRD pattern was then used to characterize the MoS_2 nanosheets. As shown in Figure S2, MoS_2 nanosheets showed the characteristic peak of pristine MoS_2 centered at $2\theta = 14.50°$, which matched with the JCPDS data of MoS_2.[37] The as-synthesized MoS_2 nanosheets had an average size of about 180 nm with certain thickness (Figure S3a) and the lattice fringe around 0.234 nm with polycrystalline structure in selective area electron diffraction (Figure S3b).

To improve the performance of MoS_2 nanosheets, lipoic acid-modified PEG-amine (LA–PEG–NH_2) is conjugated to MoS_2 surface at the defect sites. Folic acid (or folate), which is used for specific targeting of the folate receptor overexpressed on cancer cells was conjugated via LA–PEG–NH_2 linker through the EDC/NHS chemistry.[30] Different characterizations were used to confirm the successful functionalization process. Figure 1b,c shows the TEM images of MoS_2 nanosheets and MoS_2 nanosheets after PEG–FA modification. After FA–PEG modification process, the thickness of MoS_2 nanosheets obviously decreased and the average size deceased from 180 nm to about 142 nm by dynamic light scattering (DLS) analysis (Figure 1d). The decrease of thickness and size could be explained by the partial breakdown of MoS_2 nanosheets and further exfoliation during PEGylation and sonication. After FA–PEG modification, the ζ-potential of MoS_2 nanosheets shifted from −40.7 to −30.8 mV (Figure S4), indicating the presence of the PEG–FA. The conjugation of FA–PEG on MoS_2 nanosheets was then analyzed by Fourier transform infrared (FTIR) spectroscopy (Figure 1e). The peak at 472 cm^{-1} was observed in both MoS_2 and MoS_2–PEG–FA, which was attributed to the Mo–S bonding. The peaks at 640–680 and 837 cm^{-1} were attributed to the S–S characteristic stretching.[38,39] The absorption bands at 1000 and 1114 cm^{-1} were attributed to the S–O stretching.[40] The bending modes of O–H around 1635 and 3371 cm^{-1} were assigned to the water molecules. The characteristic vibration peaks within the range of 2800–3000 cm^{-1} and a weak peak at 1338 cm^{-1} were attributed to the C–H stretching of PEG and FA.[30,35] These results demonstrated the successful conjugation PEG–FA on MoS_2 nanosheets.

Thermogravimetric analysis (TGA) was also performed to show weight losses of 67.09 and 37.87% for MoS_2 and MoS_2–

DOI: 10.1021/acsami.7b18102
ACS Appl. Mater. Interfaces 2018, 10, 350–360

PEG−FA at 890 °C, respectively (Figure 2a). The gradual weight loss of MoS_2−PEG−FA between 300 and 800 °C is due to the removal of stable oxygen functional groups adhered on MoS_2 surface, indicating the attachment of PEG−FA on MoS_2. As shown in Figure 2b, the UV−vis spectra of MoS_2 nanosheets exhibited characteristic peaks around 215 and 280 nm of FA, indicating the conjugation of FA on MoS_2 nanosheets. Furthermore, X-ray photoelectron spectroscopy (XPS) measurement was performed to analyze the bonding energy information change during modification (Figure 2c). The high-resolution XPS images of Mo 3d, S 2p, and N 1s are shown in Figure 2d−f, respectively. The peaks of Mo $3d_{5/2}$ and Mo $3d_{3/2}$ in pristine MoS_2 nanosheets were 232.2 and 235.4 eV, and the two peaks shifted to 230.9 and 234 eV for MoS_2−PEG−FA, respectively. The S $2p_{5/2}$ and S $2p_{3/2}$ of pristine MoS_2 nanosheets were 163.2 and 167.8 eV and shifted to 162.8 and 165.9 eV for MoS_2−PEG−FA, respectively. Both Mo 3d and S 2p peaks showed a shift to lower binding energy due to PEG−FA conjugation. In addition, there was no N 1s peak for MoS_2 nanosheets, and the N 1s peak at 399.2 eV was observed in MoS_2−PEG−FA, which indicated the formation of CONH− between FA and PEG and the presence of N ring structure in FA.[41,42]

3.2. Stability and Biocompatibility Testing of PEG−FA Conjugation. Stable dispersion of MoS_2 nanosheets in various physiological solutions is critical for their application in biosensing. Pristine MoS_2 nanosheets might agglomerate due to restacking, leading to poor stability in solution. The layer-by-layer stacking might hide probe gene sequences and lead to the failure of hybridization between probe and target.[43] As shown in Figure 3a, it can be clearly seen that the MoS_2−PEG−FA has a better stability compared to pure MoS_2 for 4 h standing in solutions including water, PBS, and DMEM, which allowed further usage in biological and physiological environments. The size distributions of MoS_2 nanosheets before and after PEG−FA modification in the above solutions after 4 h were also measured by a DLS size analyzer. It was shown that the average size of MoS_2−PEG−FA was kept within 120−140 nm and that the average size of MoS_2 was in the micrometer range due to the possible agglomeration (Figure S5).

In real physical environment, naked oligonucleotides are easily cleaved by deoxyribonuclease I (DNase I), which directly led to the break of oligonucleotide probes and false fluorescence recovery signal.[39,44] The attachment of oligonucleotide probes on MoS_2 nanosheet surface could increase the probe stability and protect oligonucleotide probes from enzymatic degradation by DNase I. To demonstrate this, gel electrophoresis experiments with ssDNA, ssDNA−MoS_2, and ssDNA−MoS_2−PEG−FA under DNase I treatment with various time periods were performed. As shown in Figure 3b, naked ssDNA (lanes 1−3) were digested quickly and no visible signal was detected for both 5 min (lane 2) and 20 min (lane 3), which demonstrated the rapid degradation of ssDNA by DNase I. For ssDNA loaded on the MoS_2 nanosheets (lanes 4−6), ssDNA partially remained for 5 min (lane 5) and largely disappeared for 20 min (lane 6). In contrast, there was no obvious digestion in the presence of DNase I for ssDNA loaded on MoS_2−PEG−FA for both 5 min (lane 8) and 20 min (lane 9). This protection of ssDNA on MoS_2−PEG−FA may be attributed to the steric hindrance effect to prevent the enzymes absorption onto the nanocomposite surface.[45]

To study the cytotoxicity of MoS_2 nanosheets before and after PEG coating, standard MTT cell viability assays were performed for MCF-7 cells incubated with various concentrations of MoS_2 and MoS_2−PEG up to 24 h. As shown in Figure 3c, no obvious toxicity could be observed for both MoS_2 and MoS_2−PEG with cell viabilities above 80% even at high concentrations of up to 200 μg/mL. And MoS_2−PEG showed a slightly higher cell viability compared to MoS_2 nanosheets. The apoptosis degrees of MCF-7 cells incubated with MoS_2 nanosheets and MoS_2−PEG for 24 h were further quantitatively determined by flow cytometry. As shown in Figure 3d, MCF-7 cells incubated with MoS_2−PEG showed a lower apoptosis ratio of 5.80% compared to 8.47% for MoS_2, which also exhibited the slightly improved biocompatibility. Except for the cytocompatibility, hemocompatibility is another major concern for an ideal material to be used for biological application. As shown in Figure S6, no visible hemolysis effect was observed in blood for MoS_2−PEG over a concentration range of 10−100 μg/mL.

To demonstrate the specific targeting of MoS_2−PEG−FA nanoprobes on folate receptor overexpressed cancer cells, the cellular uptake experiments were performed with cancer cell lines of MCF-7 and Hela and normal cell lines of NIH3T3 and HepG2. The surface folate receptor (FR) expressions of MCF-7 cells, Hela cells, NIH3T3 cells, and HepG2 cells were first measured by Western blotting. MCF-7 cells and Hela cells had obviously higher FR expression levels compared to NIH3T3 and HepG2 cells (Figures 4a and S7). For the cellular uptake experiments, MoS_2−PEG and MoS_2−PEG−FA were incubated with each kind of cell line for 4 h. The cellular uptake levels in different kinds of cell lines were then determined by measuring Mo^{4+} content using inductively coupled plasma

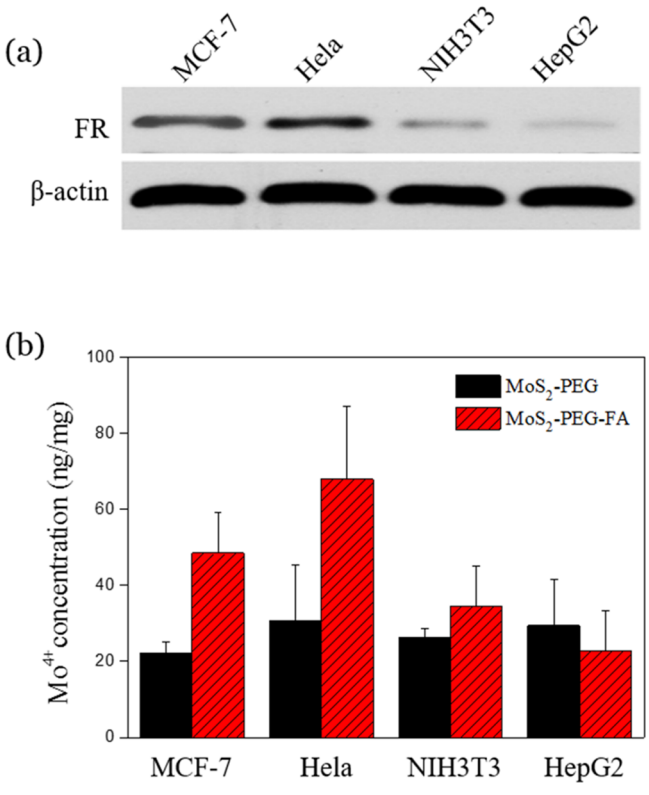

Figure 4. (a) Western blot of FR expression in Hela, MCF-7, NIH-3T3, and HepG2 cells; β-actin was used as the loading control. (b) ICP-MS for cellular uptake amount measurement of MoS_2−PEG and MoS_2−PEG−FA in cells with different FR expression levels.

DOI: 10.1021/acsami.7b18102
ACS Appl. Mater. Interfaces 2018, 10, 350−360

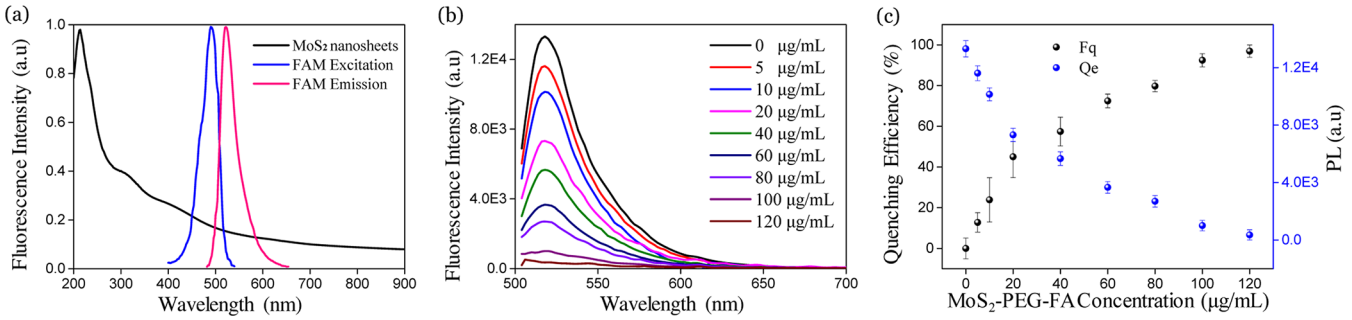

Figure 5. (a) Overlapping between adsorption spectrum of MoS_2 nanosheets and excitation and emission spectra of FAM-labeled DNA. (b) Photoluminescence spectra of FAM-labeled miRNA-21 probes incubated with MoS_2 nanosheets with a series of concentrations. (c) Quenching efficiency (%) and PL intensity of FAM-labeled miRNA-21 probe quenched by a series of concentrations of MoS_2−PEG−FA nanosheets.

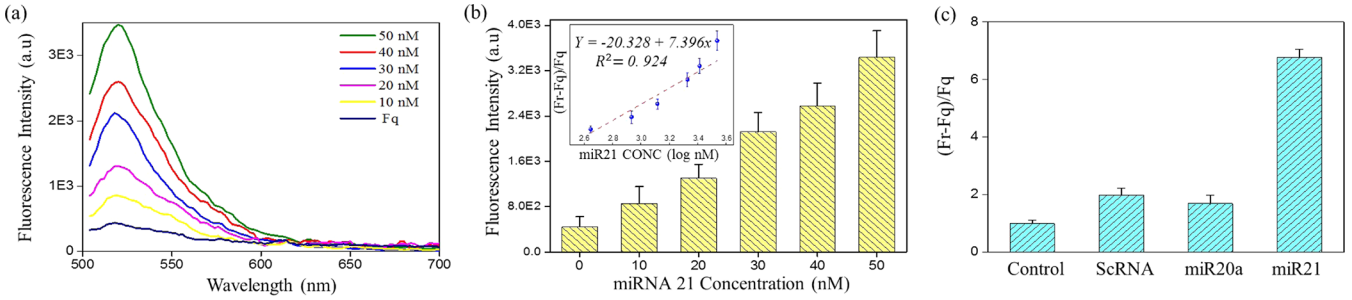

Figure 6. (a) Photoluminescence spectra of MoS_2−PEG−FA-based FRET sensing platform with the addition of miRNA-21 target with increasing concentration from 10 to 50 nM. (b) Intensity of recovered fluorescence signal with the addition of various concentrations of target miRNA-21 (inset: fitting logarithmic curve of the relative fluorescence intensity and the target miRNA-21 concentrations). (c) Comparison of relative fluorescence recovery signal for scRNA, miRNA-20a, and miRNA-21 with the same concentration of 50 nM.

mass spectrometry (ICP-MS). As shown in Figure 4b, the cellular uptakes of MoS_2−PEG for all of the four kinds of cell lines are quite similar. FA conjugation on MoS_2−PEG significantly increased the cellular uptake of nanoprobes for cancer cell lines of MCF-7 and Hela. The cellular uptakes of MoS_2−PEG−FA showed 113 and 116% increase for MCF-7 and Hela cells compared to MoS_2−PEG, respectively. In contrast, there is only a slight cellular uptake change of nanoprobes before and after FA conjugation for normal cell lines. The above experimental results demonstrated the targeting functions of MoS_2−PEG−FA on folate receptor overexpressed cancer cells.

3.3. In Vitro Sensing of miRNA-21. High quenching efficiency is the precondition for a "turn-on" FRET sensor establishment. The good matching between emission spectra of FAM-labeled probes and adsorption spectra of MoS_2 makes it possible to establish an efficient FRET system (Figure 5a). To achieve a high quenching efficiency, the ratio between the donor and acceptor molecules should be optimized. Thus, FAM-labeled probe as the donor molecule with fixed concentration (30 nM) was incubated with a series of concentrations of MoS_2−PEG−FA nanosheets ranging from 5 to 120 μg/mL. The fluorescence intensity of FAM-labeled probe of 30 nM in the same volume of PBS was considered as control signal. As shown in Figure 5b, with the increasing concentrations of MoS_2−PEG−FA, the fluorescence emission peaks of FAM-labeled probe at 520 nm decreased gradually due to the strong affinity between the nanosheets and single-stranded probes. The quenching efficiency was calculated using the equation $Q_e = (F_0 - F_q)/F_0$, where F_0 is the original fluorescence intensity of FAM-labeled probe and F_q represents the fluorescence intensity of FAM-labeled probe after quenching by MoS_2 nanosheets. As shown in Figure 5c, the quenching efficiency reached 96.95 ± 3.01% with 120 μg/mL of MoS_2 nanosheets, showing the high quenching efficiency of MoS_2 nanosheets. The quenching capabilities of MoS_2 and MoS_2−PEG−FA were also compared to the same concentration. As shown in Figure S8a, there is no obvious difference for the quenching spectra of MoS_2 and MoS_2−PEG−FA on FAM-labeled probes with the same concentration of 120 μg/mL. Both nanomaterials could achieve almost complete quenching. The quenching capabilities of MoS_2 and MoS_2−PEG−FA under various concentrations also did not show much difference (Figure S8b). Both ssDNA−MoS_2 and ssDNA−MoS_2−PEG−FA complexes showed stable quenching efficiency of above 90% in solutions over 4 h standing (Figure S8c).

The capability of the established FRET sensing platform was then tested by incubating the established ssDNA−MoS_2−PEG−FA nanoprobes with synthetic miRNA-21 at a series of concentrations from 10 to 50 nM. After incubation for 2 h at 37 °C, the recovered fluorescence signal was measured. As shown in Figure 6a, the fluorescence signal gradually enhanced with increasing concentrations of the miRNA-21 target. The fluorescence intensity peak at 520 nm showed a linear relationship with logarithmic concentration of target as the equation $y = -20.328 + 7.396x$, where y is the relatively recovered fluorescence signal $(F_r - F_q)/F_q$ and x is the logarithmic concentration of miRNA-21 (Figure 6b). Fluorescence stability of sensing against various ions, pHs, and amino acids was evaluated by PL fluorescence measurement (Figure S9), and it showed negligible change in different physiological solutions. Furthermore, to investigate the specificity of the MoS_2 nanosheet-based FRET sensor for

DOI: 10.1021/acsami.7b18102
ACS Appl. Mater. Interfaces 2018, 10, 350−360

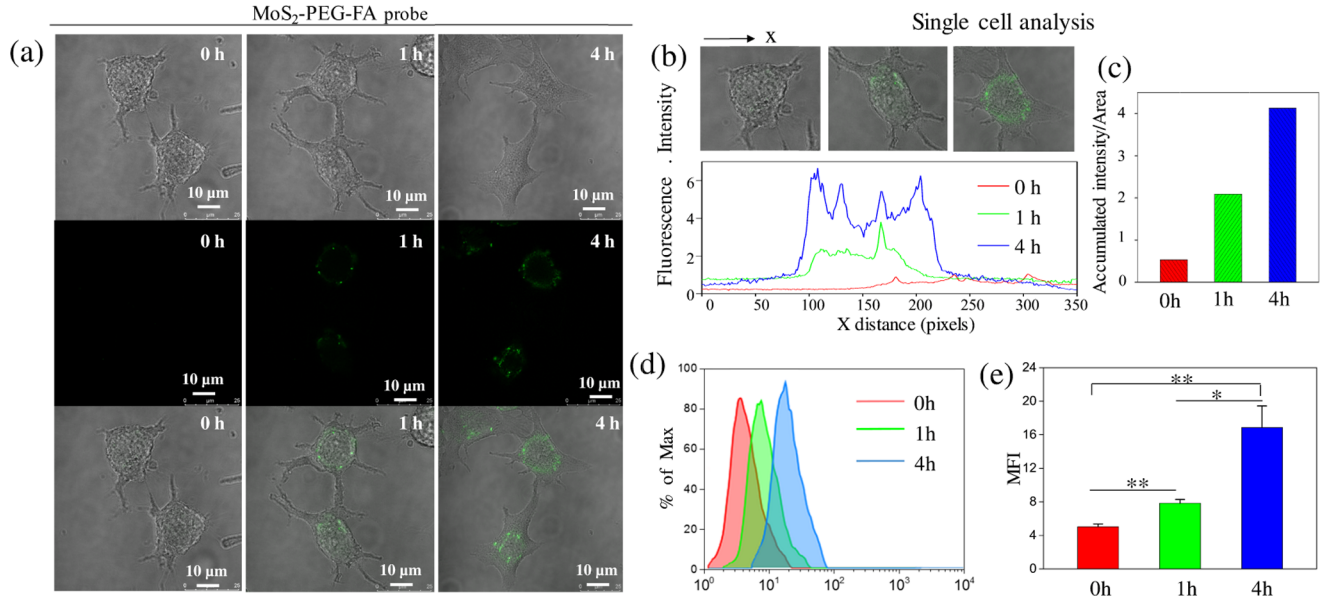

Figure 7. (a) Confocal microscopy images of MCF-7 cells incubated with ssDNA−MoS_2−PEG−FA nanoprobes for 0, 1, and 4 h. (b) Representative single-cell fluorescence image signal analysis with various incubation periods. (c) Fluorescence intensity per unit area of single cells with various incubation periods. (d) Representative histogram plots of flow cytometry showing the intracellular fluorescence recovery of MCF-7 cells upon incubation with nanoprobes. (e) Summary data of flow cytometry results (*P < 0.05, **P ≤ 0.01). The bar represents the mean fluorescence intensity (MFI) ± standard error of the mean (SEM).

miRNA-21 detection, miRNA-20a and scrambled RNA (scRNA) were tested with same procedures. Under the same concentration of 50 nM, miRNA-21 showed almost three times of signal intensity compared to scRNA and miRNA-20a, which shows obvious discrimination for intracellular sensing (Figure 6c).

3.4. Intracellular Sensing of miRNA-21. For intracellular miRNA-21 monitoring, the breast cancer MCF-7 cell, which overexpresses miRNA-21, was chosen as the cell model. In this experiment, ssDNA−MoS_2−PEG−FA probes were first incubated with MCF-7 cells for 0, 1, and 4 h. High-resolution confocal fluorescence images were then captured to analyze the fluorescence signal recovery due to the binding with miRNA-21 (Figure 7a). Single-cell fluorescence analysis was performed using ImageJ software. A gradual increase of fluorescence signal across the cell body (x-axis) was observed with increasing incubation time at single-cell level (Figure 7b). The individual cell fluorescence intensity was also normalized to individual cell area, which showed that the fluorescence intensity per unit area increased gradually with increasing incubation time (Figure 7c). This fluorescence signal recovery was due to the release of FAM−ssDNA from MoS_2 nanosheets by the stronger binding between FAM−ssDNA and endogenous miRNA-21. The previous approaches for in situ miRNA detection need long-term incubation to achieve enough internalization of nanoprobes (>10 h).[25] The above experimental results demonstrated that our ssDNA−MoS_2−PEG−FA probes could enable rapid internalization into cancer cells with overexpression of folate receptor for rapid in situ detection. The fluorescence recovery signals from multiple single cells of MCF-7 were then quantified using flow cytometry. Figure 7d showed the representative quantitative flow cytometry results of ssDNA−MoS_2−PEG−FA probes incubated with MCF-7 cells at various time points. As expected, the control cells at t = 0 h showed a low level of autofluorescence signals. The fluorescence recovery signal at 4 h showed the highest signal, which was almost 2-fold (P < 0.05) higher than that at 1 h (Figure 7e).

To examine the specificity of the MoS_2-based probes for miRNA-21 detection, human epithelial cervix carcinoma (Hela cell) was chosen as control due to its low endogenous expression of miRNA-21.[46] As demonstrated by qRT-PCR, MCF-7 cells showed a much higher miRNA-21 expression compared to Hela cells (Figure S10). In this experiment, both MCF-7 cells and Hela cells were treated with 100 μg/mL nanoprobes for 4 h under the same experimental conditions. Figure 8a shows the confocal fluorescence images of MCF-7 cells and Hela cells after 4 h incubation. MCF-7 cells showed higher fluorescence recovery signals compared to Hela cells. As shown in Figure 4b, the cellular uptake of nanoprobes for Hela cells was slightly higher than that of MCF-7 cells. This indicated that the higher fluorescence recover signals of MCF-7 cell should be mainly contributed by the higher endogenous expression of miRNA-21 rather than the internalized amount of nanoprobes. The fluorescence recovery signals from multiple single cells of MCF-7 and Hela cells were then quantified and compared using flow cytometry. Figure 8b,c shows the representative quantitative flow cytometry results of ssDNA−MoS_2−PEG−FA probes incubated with MCF-7 cells and Hela cells after 4 h incubation, respectively. The fluorescence recovery signal of MCF-7 cells was 58.7% higher than that of Hela cells after 4 h incubation (Figure 8d). The above results demonstrated a potential screening approach using the MoS_2 nanosheet-based FRET probes for rapidly and sensitively monitoring different endogenous expression levels of target miRNA at single-cell level.

4. CONCLUSIONS

In this work, MoS_2 nanosheet-based FRET probes were developed for measuring miRNA-21 expression in living cancer cells. This miRNA sensing strategy is based on monitoring fluorescence "off−on" change of internalized ssDNA−MoS_2−

DOI: 10.1021/acsami.7b18102
ACS Appl. Mater. Interfaces 2018, 10, 350−360

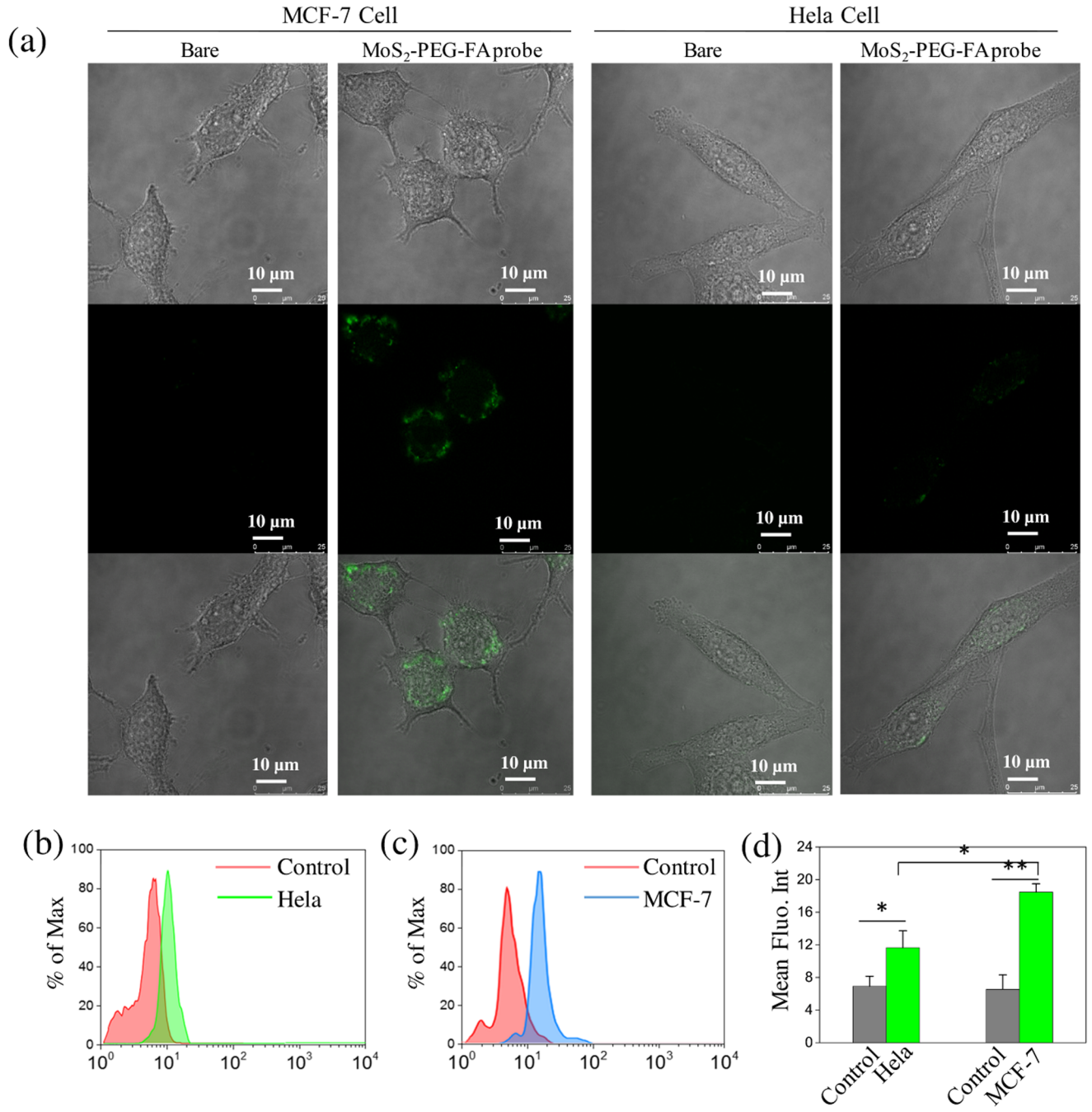

Figure 8. (a) Confocal microscopy images of MCF-7 cells and Hela cells incubated with ssDNA−MoS_2−PEG−FA nanoprobes for 4 h. (b, c) Representative histogram plots of flow cytometry showing the intracellular fluorescence recovery upon incubation with nanoprobes for MCF-7 cells and Hela cells, respectively. (d) Summary data of flow cytometry results for Hela cells and MCF-7 cells for 4 h incubation. The bar represents the mean fluorescence intensity (MFI) ± SEM.

PEG−FA probes due to the hybridization of endogenous miRNA with FAM−ssDNA. PEG-folate-modified MoS_2 nanosheets provided excellent biocompatibility, probe gene protection, and cancer cell targeting function. The results of miRNA-21 expression detection in living MCF-7 and Hela cells demonstrated the feasibility of this MoS_2-based nanoprobes for in situ single-step miRNA detection at the single-cell level, which could be a promising single-cell analysis platform to monitor miRNA expression for fundamental research and clinical applications.

■ ASSOCIATED CONTENT

Supporting Information

The Supporting Information is available free of charge on the ACS Publications website at DOI: 10.1021/acsami.7b18102.

Calibration curve of Mo^{4+} for ICP-MS; XRD patterns of pristine MoS_2 and MoS_2 nanosheets; high-resolution TEM image of pristine MoS_2 nanosheets; ζ potential measurement; hemolysis activity testing; gray intensity analysis of Western blotting results; quenching stability testing; fluorescence stability testing against various ions, pH, and amino acids; and qRT-PCR results (PDF)

DOI: 10.1021/acsami.7b18102
ACS Appl. Mater. Interfaces 2018, 10, 350−360

AUTHOR INFORMATION

Corresponding Authors

*E-mail: chunyi.wen@polyu.edu.hk. Phone: +852-34008898. Fax: +852-23342429 (C.W.).

*E-mail: Mo.Yang@polyu.edu.hk. Phone: +852-27664946. Fax: +852-23342429 (M.Y.).

ORCID

Mo Yang: 0000-0002-3863-8187

Notes

The authors declare no competing financial interest.

ACKNOWLEDGMENTS

This work was supported by the National Natural Science Foundation of China (NSFC) (Grant Nos. 81471747 and 31771077), the Hong Kong Research Council General Research Grant (PolyU 152213/15E), and the Hong Kong Polytechnic University Internal Fund (1-ZVJ7). This work was also supported by the University Research Facility in Life Sciences of the Hong Kong Polytechnic University.

ABBREVIATIONS

FA, folic acid; FRET, fluorescence resonance energy transfer; MoS_2, molybdenum disulfide; ssDNA, single-stranded DNA; PEG, poly(ethylene glycol)

REFERENCES

(1) Ambros, V. The Functions of Animal microRNAs. *Nature* **2004**, *431*, 350−355.

(2) Bartel, D. P. MicroRNAs: Genomics, Biogenesis, Mechanism, and Function. *Cell* **2004**, *116*, 281−297.

(3) Dong, H.; Lei, J.; Ding, L.; Wen, Y.; Ju, H.; Zhang, X. MicroRNA: Function, Detection, and Bioanalysis. *Chem. Rev.* **2013**, *113*, 6207−6233.

(4) Ma, J.; Dong, C.; Ji, C. MicroRNA and Drug Resistance. *Cancer Gene Ther.* **2010**, *17*, 523−531.

(5) Kutanzi, K. R.; Yurchenko, O. V.; Beland, F. A.; Vasyl'F, C.; Pogribny, I. P. MicroRNA-Mediated Drug Resistance in Breast Cancer. *Clin. Epigenet.* **2011**, *2*, 171−185.

(6) Xu, Q.; Ma, F.; Huang, S.-Q.; Tang, B.; Zhang, C.-Y. Nucleic Acid Amplification-Free Bioluminescent Detection of microRNAs with High Sensitivity and Accuracy Based on Controlled Target Degradation. *Anal. Chem.* **2017**, *89*, 7077−7083.

(7) Yan, L. X.; Wu, Q. N.; Zhang, Y.; Li, Y. Y.; Liao, D. Z.; Hou, J. H.; Fu, J.; Zeng, M. S.; Yun, J. P.; Wu, Q. L.; et al. Knockdown of miR-21 in Human Breast Cancer Cell Lines Inhibits Proliferation, in Vitro Migration and in Vivo Tumor Growth. *Breast Cancer Res.* **2011**, *13*, No. R2.

(8) Calin, G. A.; Croce, C. M. MicroRNA Signatures in Human Cancers. *Nat. Rev. Cancer* **2006**, *6*, 857−866.

(9) Graybill, R. M.; Bailey, R. C. Emerging Biosensing Approaches for microRNA Analysis. *Anal. Chem.* **2016**, *88*, 431−450.

(10) Kim, S. W.; Li, Z.; Moore, P. S.; Monaghan, A. P.; Chang, Y.; Nichols, M.; John, B. A Sensitive Non-Radioactive Northern Blot Method to Detect Small RNAs. *Nucleic Acids Res.* **2010**, *38*, No. e98.

(11) Várallyay, É; Burgyán, J.; Havelda, Z. MicroRNA Detection by Northern Blotting Using Locked Nucleic Acid Probes. *Nat. Protoc.* **2008**, *3*, 190−196.

(12) Liu, C.-G.; Calin, G. A.; Volinia, S.; Croce, C. M. MicroRNA Expression Profiling Using Microarrays. *Nat. Protoc.* **2008**, *3*, 563−578.

(13) Tian, T.; Wang, J.; Zhou, X. A Review: MicroRNA Detection Methods. *Org. Biomol. Chem.* **2015**, *13*, 2226−2238.

(14) Deng, Y.; Wang, C. C.; Choy, K. W.; Du, Q.; Chen, J.; Wang, Q.; Li, L.; Chung, T. K. H.; Tang, T. Therapeutic Potentials of Gene Silencing by RNA Interference: Principles, Challenges, and New Strategies. *Gene* **2014**, *538*, 217−227.

(15) Ma, F.; Liu, M.; Tang, B.; Zhang, C.-Y. Rapid and Sensitive Quantification of microRNAs by Isothermal Helicase-Dependent Amplification. *Anal. Chem.* **2017**, *89*, 6182−6187.

(16) Dong, M.; Tepp, W. H.; Johnson, E. A.; Chapman, E. R. Using Fluorescent Sensors to Detect Botulinum Neurotoxin Activity in Vitro and in Living Cells. *Proc. Natl. Acad. Sci. U.S.A.* **2004**, *101*, 14701−14706.

(17) Ma, F.; Li, Y.; Tang, B.; Zhang, C.-Y. Fluorescent Biosensors Based on Single-Molecule Counting. *Acc. Chem. Res.* **2016**, *49*, 1722−1730.

(18) Zhu, G.; Liang, L.; Zhang, C.-Y. Quencher-Free Fluorescent Method for Homogeneously Sensitive Detection of microRNAs in Human Lung Tissues. *Anal. Chem.* **2014**, *86*, 11410−11416.

(19) Zhou, J.; Yang, Y.; Zhang, C.-Y. Toward Biocompatible Semiconductor Quantum Dots: From Biosynthesis and Bioconjugation to Biomedical Application. *Chem. Rev.* **2015**, *115*, 11669−11717.

(20) Wang, Q.; Wang, W.; Lei, J.; Xu, N.; Gao, F.; Ju, H. Fluorescence Quenching of Carbon Nitride Nanosheet through Its Interaction with DNA for Versatile Fluorescence Sensing. *Anal. Chem.* **2013**, *85*, 12182−12188.

(21) Shi, J.; Lyu, J.; Tian, F.; Yang, M. A Fluorescence Turn-On Biosensor Based on Graphene Quantum Dots (GQDs) and Molybdenum Disulfide (MoS_2) Nanosheets for Epithelial Cell Adhesion Molecule (EpCAM) Detection. *Biosens. Bioelectron.* **2017**, *93*, 182−188.

(22) Shi, J.; Guo, J.; Bai, G.; Chan, C.; Liu, X.; Ye, W.; Hao, J.; Chen, S.; Yang, M. A Graphene Oxide Based Fluorescence Resonance Energy Transfer (FRET) Biosensor for Ultrasensitive Detection of Botulinum Neurotoxin A (BoNT/A) Enzymatic Activity. *Biosens. Bioelectron.* **2015**, *65*, 238−244.

(23) Tian, F.; Lyu, J.; Shi, J.; Yang, M. Graphene and Graphene-Like Two-Denominational Materials Based Fluorescence Resonance Energy Transfer (FRET) Assays for Biological Applications. *Biosens. Bioelectron.* **2017**, *89*, 123−135.

(24) Ryoo, S.-R.; Lee, J.; Yeo, J.; Na, H.-K.; Kim, Y.-K.; Jang, H.; Lee, J. H.; Han, S. W.; Lee, Y.; Kim, V. N.; et al. Quantitative and Multiplexed microRNA Sensing in Living Cells Based on Peptide Nucleic Acid and Nano Graphene Oxide (PANGO). *ACS Nano* **2013**, *7*, 5882−5891.

(25) Esteban-Fernández de Ávila, B.; Martín, A.; Soto, F.; Lopez-Ramirez, M. A.; Campuzano, S.; Vásquez-Machado, G. M.; Gao, W.; Zhang, L.; Wang, J. Single cell Real-Time miRNAs Sensing Based on Nanomotors. *ACS Nano* **2015**, *9*, 6756−6764.

(26) Liao, X.; Wang, Q.; Ju, H. Simultaneous Sensing of Intracellular microRNAs with A Multi-Functionalized Carbon Nitride Nanosheet Probe. *Chem. Commun.* **2014**, *50*, 13604−13607.

(27) Tsang, M.-K.; Ye, W.; Wang, G.; Li, J.; Yang, M.; Hao, J. Ultrasensitive Detection of Ebola Virus Oligonucleotide Based on Upconversion Nanoprobe/Nanoporous Membrane System. *ACS Nano* **2016**, *10*, 598−605.

(28) Jia, L.; Ding, L.; Tian, J.; Bao, L.; Hu, Y.; Ju, H.; Yu, J.-S. Aptamer Loaded MoS_2 Nanoplates as Nanoprobes for Detection of Intracellular ATP and Controllable Photodynamic Therapy. *Nanoscale* **2015**, *7*, 15953−15961.

(29) Kou, Z.; Wang, X.; Yuan, R.; Chen, H.; Zhi, Q.; Gao, L.; Wang, B.; Guo, Z.; Xue, X.; Cao, W.; et al. A Promising Gene Delivery System Developed From PEGylated MoS_2 Nanosheets for Gene Therapy. *Nanoscale Res. Lett.* **2014**, *9*, No. 587.

(30) Liu, T.; Wang, C.; Gu, X.; Gong, H.; Cheng, L.; Shi, X.; Feng, L.; Sun, B.; Liu, Z. Drug Delivery with PEGylated MoS_2 Nano-Sheets for Combined Photothermal and Chemotherapy of Cancer. *Adv. Mater.* **2014**, *26*, 3433−3440.

(31) Zhu, C.; Zeng, Z.; Li, H.; Li, F.; Fan, C.; Zhang, H. Single-Layer MoS_2-Based Nanoprobes for Homogeneous Detection of Biomolecules. *J. Am. Chem. Soc.* **2013**, *135*, 5998−6001.

(32) Kim, H. Y.; Li, F.; Park, J. Y.; Kim, D.; Park, J. H.; Han, H. S.; Byun, J. W.; Lee, Y.-S.; Jeong, J. M.; Char, K.; et al. In Vivo

DOI: 10.1021/acsami.7b18102
ACS Appl. Mater. Interfaces 2018, 10, 350−360

Visualization of Endogenous miR-21 Using Hyaluronic Acid-Coated Graphene Oxide for Targeted Cancer Therapy. *Biomaterials* **2017**, *121*, 144−154.
(33) Teo, W. Z.; Chng, E. L. K.; Sofer, Z.; Pumera, M. Cytotoxicity of Exfoliated Transition-Metal Dichalcogenides (MoS_2, WS_2, and WSe_2) is Lower Than That of Graphene and its Analogues. *Chem. - Eur. J.* **2014**, *20*, 9627−9632.
(34) Zhou, J.; Romero, G.; Rojas, E.; Moya, S.; Ma, L.; Gao, C. Folic Acid Modified Poly (Lactide-Co-Glycolide) Nanoparticles, Layer-by-Layer Surface Engineered for Targeted Delivery. *Macromol. Chem. Phys.* **2010**, *211*, 404−411.
(35) Feng, W.; Chen, L.; Qin, M.; Zhou, X.; Zhang, Q.; Miao, Y.; Qiu, K.; Zhang, Y.; He, C. Flower-Like PEGylated MoS_2 Nanoflakes for Near-Infrared Photothermal Cancer Therapy. *Sci. Rep.* **2015**, *5*, No. 17422.
(36) Yu, J.; Yin, W.; Zheng, X.; Tian, G.; Zhang, X.; Bao, T.; Dong, X.; Wang, Z.; Gu, Z.; Ma, X. Smart MoS_2/Fe_3O_4 Nanotheranostic for Magnetically Targeted Photothermal Therapy Guided by Magnetic Resonance/Photoacoustic Imaging. *Theranostics* **2015**, *5*, 931−945.
(37) Ding, S.; Zhang, D.; Chen, J. S.; Lou, X. W. D. Facile Synthesis of Hierarchical MoS_2 Microspheres Composed of Few-Layered Nanosheets and Their Lithium Storage Properties. *Nanoscale* **2012**, *4*, 95−98.
(38) Vattikuti, S. V. P.; Byon, C. Synthesis and Characterization of Molybdenum Disulfide Nanoflowers and Nanosheets: Nanotribology. *J. Nanomater.* **2015**, *2015*, No. 710462.
(39) Lu, C.-H.; Zhu, C.-L.; Li, J.; Liu, J.-J.; Chen, X.; Yang, H.-H. Using Graphene to Protect DNA from Cleavage During Cellular Delivery. *Chem. Commun.* **2010**, *46*, 3116−3118.
(40) Pua, F. L.; Chia, C. H.; Zakari, S.; Liew, T. K.; Yarmo, M. A.; Huang, N. M. Preparation of Transition Metal Sulfide Nanoparticles via Hydrothermal Route. *Sains Malays.* **2010**, *39*, 243−248.
(41) Cipreste, M. F.; Gonzalez, I.; da Mata Martins, T. M.; Goes, A. M.; de Almeida Macedo, W. A.; de Sousa, E. M. B. Attaching Folic Acid on Hydroxyapatite Nanorod Surfaces: An Investigation of the HA−FA Interaction. *RSC Adv.* **2016**, *6*, 76390−76400.
(42) Zhao, L.; Kim, T.-H.; Ahn, J.-C.; Kim, H.-W.; Kim, S. Y. Highly Efficient "Theranostics" System Based on Surface-Modified Gold Nanocarriers for Imaging and Photodynamic Therapy of Cancer. *J. Mater. Chem. B* **2013**, *1*, 5806−5817.
(43) Liu, K.; Zhang, J.-J.; Cheng, F.-F.; Zheng, T.-T.; Wang, C.; Zhu, J.-J. Green and Facile Synthesis of Highly Biocompatible Graphene Nanosheets and its Application for Cellular Imaging and Drug Delivery. *J. Mater. Chem.* **2011**, *21*, 12034−12040.
(44) Yang, Y.; Huang, J.; Yang, X.; Quan, K.; Wang, H.; Ying, L.; Xie, N.; Ou, M.; Wang, K. FRET Nanoflares for Intracellular mRNA Detection: Avoiding False Positive Signals and Minimizing Effects of System Fluctuations. *J. Am. Chem. Soc.* **2015**, *137*, 8340−8343.
(45) Wang, H.; Yang, R.; Yang, L.; Tan, W. Nucleic Acid Conjugated Nanomaterials for Enhanced Molecular Recognition. *ACS Nano* **2009**, *3*, 2451−2460.
(46) Tomaselli, S.; Galeano, F.; Alon, S.; Raho, S.; Galardi, S.; Polito, V. A.; Presutti, C.; Vincenti, S.; Eisenberg, E.; Locatelli, F.; et al. Modulation of microRNA Editing, Expression and Processing by $ADAR_2$ Deaminase in Glioblastoma. *Genome Biol.* **2015**, *16*, No. 5.

DOI: 10.1021/acsami.7b18102
ACS Appl. Mater. Interfaces 2018, 10, 350−360